2019-04-03

GEANT4 simulation of fast neutron interactions in detectors based on Bismuth Germanate (Bi4Ge3O12)

Batteson, Bruce; Smith, Craig F.; Verbeke, Jerome M.

Lawrence Livermore National Labratory

Batteson, B., C. F. Smith, and J. M. Verbeke. GEANT4 simulation of fast neutron interactions in detectors based on Bismuth Germanate (Bi4Ge3O12). No. LLNL-CONF-771059. Lawrence Livermore National Lab.(LLNL), Livermore, CA (United States), 2019.

https://hdl.handle.net/10945/62864

LLNL-CONF-771059

LAWRENCE
LIVERMORE
NATIONAL
LABORATORY

GEANT4 simulation of fast neutron interactions in detectors based on Bismuth Germanate (Bi4Ge3O12)

B. Batteson, C. F. Smith, J. M. Verbeke

April 3, 2019

Hardened Electronics and Radiation Technology
San Diego, CA, United States
April 8, 2019 through April 12, 2019

Disclaimer

GEANT4 simulation of fast neutron interactions in detectors based on Bismuth Germanate ($Bi_4Ge_3O_{12}$)

Bruce Batteson
Naval Postgraduate School, Monterey CA
bruce.batteson@nps.edu

Bruce Batteson, Naval Postgraduate School, Monterey CA
Craig F. Smith, Naval Postgraduate School, Monterey CA
Jerome M. Verbeke, Lawrence Livermore National Laboratory, Livermore, CA

Unlimited Release 35 words or less abstract:

We have developed a GEANT4 model of neutron detectors based on Bismuth Germanate (BGO) to improve understanding of their performance especially in their potential application to the detection of special nuclear materials.

Classification level of final presentation/poster: ☒ Unclassified ☐ Classified

Presentation Preference: ☒ Oral ☐ Poster ☐ Computer Demo

Computer Demonstration Objective: (leave blank if not requesting computer demonstration)

Sponsor/Approver: DTRA-NSERC

GEANT4 simulation of fast neutron interactions in detectors based on Bismuth Germanate ($Bi_4Ge_3O_{12}$)

Bruce Batteson
Craig F. Smith
Naval Postgraduate School

Jerome M. Verbeke
Lawrence Livermore National Laboratory

I. INTRODUCTION

FAST neutron detection is critical to the interdiction of illicit special nuclear material (SNM). Currently-fielded ^{3}He detectors typically rely on moderating material such as water or plastic to slow incident neutrons to thermal levels where they can interact with ^{3}He and thus be registered in the detector. However, such moderation substantially increases the size of the detector and limits the efficiency of detection.

The low efficiency of current ^{3}He-based detectors against fast neutron sources combined with shortages of raw ^{3}He have spurred recent work in alternative detector technologies. Many avenues are being pursued but one of the most promising is the use of heavy oxide scintillators (e.g., $Bi_4Ge_3O_{12}$, Gd_2SiO_5Ce and $ZnWO_4$) to detect fast neutrons [1]. This method requires little to no moderation and enables construction of highly efficient, compact (man-portable), and rugged detectors.

In this work, we are using the GEANT4 simulation toolkit in order to simulate response of heavy oxide scintillator materials to incident neutrons such as those produced by SNM. GEANT4 is a toolkit originating at CERN and developed in a worldwide collaboration. It is used to simulate the physics processes of particles passing through matter [2]. In conjunction with GEANT4, we are using the LEND physics list developed by Lawrence Livermore National Laboratory[1]. Data is collected and analyzed using ROOT based on the physics process (as defined by the LEND physics list) and incident energy.

ROOT is a toolkit created at CERN for storage and statistical analysis of large amounts of data [3].

II. PURPOSE OF WORK

Previous work has demonstrated the potential of heavy oxide scintillators (e.g., $Bi_4Ge_3O_{12}$, Gd_2SiO_5Ce and $ZnWO_4$) as a suitable material for detection of fast neutrons, in particular to enable interdiction of illicit SNM. Experiments have demonstrated fast neutron detection efficiency near 50% for single crystal detectors as well as ZEBRA detectors (multilayer detectors with composite heavy oxide scintillators) based on $Bi_4Ge_3O_{12}$, Gd_2SiO_5Ce and $ZnWO_4$ [4].

Various physical modes of optical photon production exist in these materials and are qualitatively described in previous work [1]. Our work, the start of which is presented here, quantifies the relative contribution of each of these physical modes to overall detection in these materials. Such quantization will enable optimization of detector design and increase fidelity in interpretation of detector response.

III. THEORETICAL CONSIDERATIONS

A brief review of the Evaluated Nuclear Data File (ENDF) for ^{209}Bi reveals many potential neutron interactions [5]. Being neutral particles, neutrons do not directly produce a scintillation response in the scintillation material. Instead, the interaction of neutrons within the detector cause a variety of processes to occur with corresponding impacts (e.g., recoil, ionization, nuclear excitation) which ultimately trigger the production of scintillation photons within the detector.

Ryzhikov et al. postulate that the neutron interaction modes with the greatest impact on detector performance are elastic and inelastic scattering and resonant and thermal capture, and that other interactions, such as

[1] The LEND physics list will become available in the public GEANT4 distribution in the near future. Interested parties can contact Douglas Wright at wright20@llnl.gov.

$(n, 2n)$, have a much lesser contribution [1].

A. Elastic Scattering

Elastic scattering of neutrons in ^{209}Bi is a significant mode for energies below 1 MeV. Since the energy transfer in elastic scattering is inversely proportional to the atomic number of the target nucleus, elastic scattering is not a significant precursor to optical photon production in ^{209}Bi. However, in BGO, elastic scattering with the ^{16}O nuclei produces gamma quanta when the ^{16}O nuclei de-excite as shown in equation (1).

$$A + n \rightarrow A^{*} + n' \rightarrow A + n' + \gamma \qquad (1)$$

B. Inelastic scattering

Inelastic scattering in ^{209}Bi is a significant mode of interaction for neutrons with energies above 1 MeV. At these energies, the neutron and target nucleus form an excited compound nucleus which then decays, emitting the scattered neutron [1]. Gamma quanta are emitted both by de-excitation of the intermediate compound nucleus and of the final nucleus as in equation (2).

$$A + n \rightarrow (A+1)^{*} \rightarrow (A+1) + \gamma_1 \rightarrow A^{*} + n' \rightarrow A + n' + \gamma_2 \qquad (2)$$

C. Neutron capture

Resonant neutron capture is a significant mode of interaction for neutrons with energies below 1 MeV. Capture occurs when the incident neutron energy matches an excited state of the compound nucleus as in equation (3). The excited state then decays, producing gamma quanta.

Thermal neutron capture occurs when incident neutron energy approaches the energies corresponding to ambient temperatures (around 0.025 eV). Although thermal neutron capture has a significantly higher cross section than inelastic scattering, the low levels of thermal neutrons in the unmoderated spectra of SNM limit the number of such interactions that are expected to result.

$$A + n \rightarrow (A+1)^{*} \rightarrow (A+1) + \gamma \qquad (3)$$

D. Neutron pair production

Neutron pair production $(n, 2n)$ is a significant mode of interaction for energies above 10 MeV. Although this reaction does not directly result in a detectable signal, it increases the number of neutrons available for subsequent reactions.

E. Other reactions

There are a number of other possible neutron interactions such as proton, deuteron, triton, and alpha production which can also ultimately result in optical photons. However, these reactions contribute significantly less to the detectable signal due to the small cross sections.

IV. Simulation Design

A. Simulation strategy

The overarching strategy of the simulation is to associate every optical photon produced with a preceding neutron interaction in order to quantify the relative contribution of each neutron reaction channel to the detectable signal. Note that several interactions may occur between the neutron interaction and the production of the optical photon but we are primarily interested in the neutron interaction at the beginning of this reaction chain.

Neutron interactions are categorized by the physics process as defined in the LEND physics list within GEANT4. LEND neutron reaction channels include elastic, capture, fission, and other. In order to improve fidelity on the reactions labeled 'other', our simulation further categorizes reactions by their progeny in order to correlate the reaction subtype with the ENDF reaction type number.

Within GEANT4, optical photons are treated as a particle distinct from gamma photons. Optical photons are produced in the simulation by scintillation following a statistical distribution which is encoded as one of several macroscopic optical properties. Although our simulation does allow production of optical photons through Cerenkov radiation, it has a negligible affect since we are primarily interested in neutron radiation. Other optical properties encoded in the simulation include the refractive index distribution, absorption distribution, and scintillation yield. Optical surfaces are defined at the boundaries of the target using the BGO look up tables distributed with GEANT4.

B. Simulation Limitations

Sources are modelled as pure neutron sources without associated gamma spectra. This is intentional since our focus is primarily on response to neutron radiation and can be thought of as a detector perfectly shielded from gamma radiation.

GEANT4 interpolates the scintillation emission spectra as the mean of the values of two adjacent points. This gives the optical photon emission spectra an uncharacteristic stepped form. We have mitigated this effect by providing a large number of data points for the characteristic emission spectra [6].

Although it does not adversely affect our simulation, it is worth noting that GEANT4 does not enforce conservation of energy in the creation of optical photons[7].

C. Simulation geometry

We have built a simple simulation geometry consisting of a monolithic cylindrical target 19.86 mm in diameter and 9.97 mm deep exposed to a unidirectional neutron source. The target sides and the face presented to the source are wrapped in Teflon. The remaining face is considered the detection face which would in practice be coupled to a photomultiplier tube. Optical photons arriving at this face are considered detected.

The neutron source is simulated as a general particle source 1m from the target. To facilitate cross section comparison, we modelled an isotropic planar source with the same cross section as the frontal area of the target. The BGO target was simulated with elemental makeup as listed in Table 1.

TABLE 1
Isotopic abundance in simulated detector material (BGO)

Element	Isotope	Mass fraction
Bi		67.10 %
	^{209}Bi	67.10 %
Ge		17.49 %
	^{70}Ge	3.64 %
	^{72}Ge	4.82 %
	^{73}Ge	1.35 %
	^{74}Ge	6.35 %
	^{76}Ge	1.33 %
O		15.41 %
	^{16}O	15.37 %
	^{17}O	0.00586 %
	^{18}O	0.0316 %

V. SIMULATION RESULTS

To date, we have run four simulations. The first two simulations compare cross section and resonant capture observed in our simulation to expected values in order to verify the validity of the simulation design. The third and fourth simulations model ^{252}Cf and ^{239}Pu-Be neutron sources to quantize the optical photon production due to each neutron reaction mode. Each simulation ran 10 million events, each event consisting of a single incident neutron. All simulations are at standard conditions.

A. Cross section validation

Our first validation was to compare the simulation results to accepted cross sections by simulating a 14.1MeV isotropic neutron source against a ^{209}Bi target. We calculated the resulting cross section and compared it to the accepted values from ENDF/BVII [5]. The simulation results are generally within the standard counting error of the accepted values. However, the simulation cross section for $(n, 2n)$ is 1.5 standard deviations from the expected value and this discrepancy in turn results in a higher (n, tot) cross section. Additional work is required to determine the root cause of this discrepancy.

TABLE 2
Comparison to ENDF cross sections. Although generally in close agreement, the simulated cross section is not within one standard counting error of the expected value for (n,tot) and (n,2n) reactions. Further work is required to determine the root cause of this discrepancy. Standard error in parenthesis.

Process	Simulation Cross Section	ENDF Cross Section [5]	Diff. (%)
(n,tot)	5.408 (0.004926)	5.36	0.901
(n,el)	2.819 (0.04542)	2.823	-0.137
(n,n')	0.392 (0.008742)	0.3862	1.5
(n,g)	0.0009582 (0.000401)	0.00102	-6.06
(n,2n)	2.192 (0.03225)	2.144	2.22
(n,p)	0.0009659 (0.0004026)	0.0009283	4.05
(n,p n)	0.002598 (0.0006604)	0.002723	-4.62
(n,d)	0.0002117 (0.0001884)	0.0002274	-6.94
(n,t)	5.772e-05 (9.841e-05)	6.92e-05	-16.6
(n,a)	0.0007773 (0.0003612)	0.0007368	5.5
(n,a n)	8.081e-05 (0.0001164)	7.492e-05	7.87

B. Resonant capture validation

Our second validation was to compare our simulation behavior with experimentally observed resonant energies by simulating an isotropic neutron source with a linear energy distribution from 0.01 to 5 keV and a ^{209}Bi target. Our simulation shows resonant peaks at various energies across the spectrum (Fig. 1). As seen in

Table 3, four of the peaks observed in the simulation of neutron capture by BGO (792.22 eV, 2332.98 eV, 3343.34 eV, and 4459.26 eV) are within 1.2% of resonant energies experimentally observed in ^{209}Bi by the CERN neutron Time of Flight (nTOF) collaboration [8]. The twin peaks centered around 800 eV in the simulation output closely match the twin peaks observed in the experimental data. However the two distinct peaks centered about 2307 eV are not observed in the experimental data, which has a single although slightly broadened peak at 2323.8 eV [8]. Further analysis is necessary to determine the origin of these peaks.

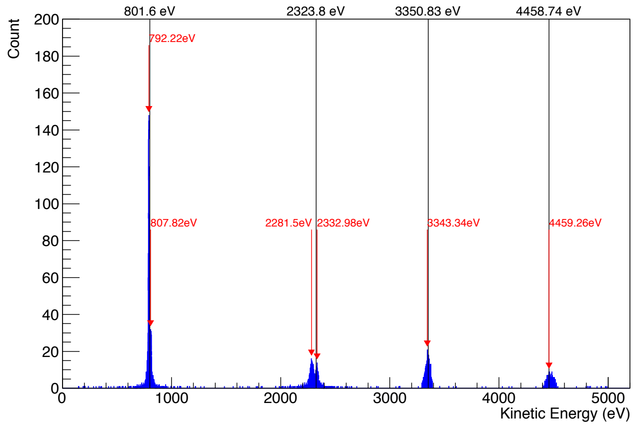

Fig. 1. Simulation of a linear spectrum of 1×10^7 neutrons from 0.01 eV to 5 keV incident on ^{209}Bi resulted in 7479 capture events. Resonant neutron capture occurs when the incident neutron energy corresponds to an excited state of the target nucleus. Simulation in GEANT4 reproduced resonance peaks (shown in red) at 792.22 eV, 807.82 eV, 2281.5 eV, 2332.98 eV, 3343.34 eV, and 4459.26 eV which closely match those measured at the CERN nTOF facility (shown in black) at 801.6 eV, 2323.8 eV, 3350.83 eV, and 4458.74 eV [8].

TABLE 3

Comparison of resonant neutron capture by BGO as observed in simulation against experimental data of resonant neutron capture by ^{209}Bi.

Resonant energies observed in simulation	Resonant energies observed experimentally [8]	Difference
792.22 eV	801.6 eV	9.38 eV 1.17 %
2332.98 eV	2323.8 eV	9.18 eV 0.395 %
3343.34 eV	3350.83 eV	7.49 eV 0.224 %
4459.26 eV	4458.74 eV	0.52 eV 0.0117 %

C. *Response to ^{252}Cf neutron spectrum*

Our third simulation examined the response to a ^{252}Cf point neutron source. We recorded the number of optical photons resulting from each neutron reaction mode and compare the fraction of neutron reactions to fraction of optical photons produced. From the results shown in Fig. 2, we observe that the production of optical photons is predominantly due to elastic and inelastic scattering of incident neutrons. Although inelastic scattering accounts for only 12.7% of all neutron reactions, it accounts for 46.2% of optical photon production. Similarly, we observe that (n, α), (n, p), $(n, 2n)$, and neutron capture produce significantly more optical photons than is suggested by the overall fraction of each neutron reaction.

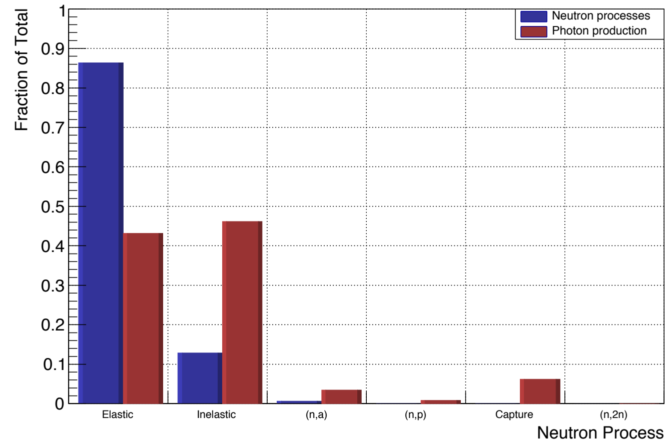

Fig. 2. Simulation of a ^{252}Cf neutron source incident on BGO. Although inelastic scattering accounts for only 12.7% of all neutron reactions, it accounts for 46.2% of optical photon production. Similarly, we observe that (n, α), (n, p), $(n, 2n)$, and neutron capture produce significantly more optical photons than is suggested by the overall fraction of each neutron reaction.

D. *Response to ^{239}Pu-Be neutron spectrum*

Our fourth simulation examined the response to a ^{239}Pu-Be point neutron source. As before, we recorded the number of optical photons resulting from each neutron reaction mode and compare the fraction of neutron reactions to fraction of optical photons produced. From the results shown in Fig. 3, we observe that the production of optical photons is predominantly due to inelastic scattering of incident neutrons. Although inelastic scattering accounts for only 24.2% of all neutron reactions, it accounts for 81.1% of optical photon production. Similarly, we observe that (n, α), (n, p), and neutron capture on average each produce significantly more optical photons than is suggested by the overall fraction of each neutron reaction.

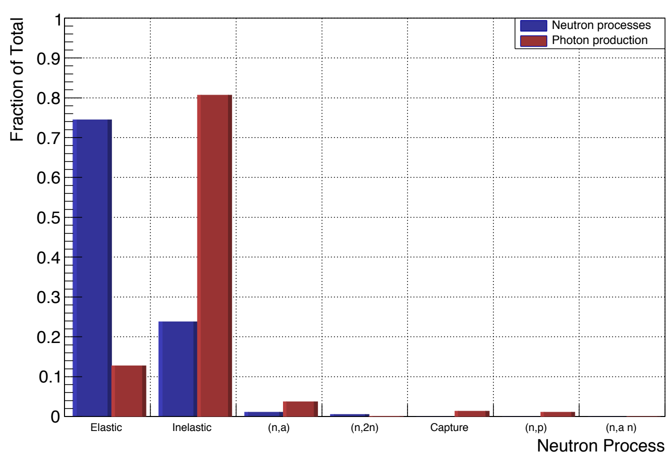

Fig. 3. Simulation of a ^{239}Pu-Be neutron source incident on BGO. Although inelastic scattering accounts for only 24.2% of all neutron reactions, it accounts for 81.1% of optical photon production. Similarly we observe (n, α), (n, p), and neutron capture produce significantly more optical photons than is suggested by the overall fraction of each neutron reaction.

VI. CONCLUSION

Our simulation requires further development, but the correlation between our initial results and previous experimental data confirms the validity of the simulation design.

Our initial analysis of photon production provides quantified data to support the theoretical and experimental results of Ryzhikov et al [1]. As expected, the production of optical photons cannot be directly correlated to the cross section of each neutron reaction. Optical photon production is predominantly due to inelastic scattering. Other neutron reactions such as (n, α), (n, p), $(n, 2n)$, and neutron capture produce significantly more optical photons than suggested by the cross section of each neutron reaction.

Future work will include modelling more complex detector geometries such as the multilayer ZEBRA composite material [1] and incorporating complex neutron-gamma sources.

VII. ACKNOWLEDGMENT

Lawrence Livermore National Laboratory is operated by Lawrence Livermore National Security, LLC, for the U.S. Department of Energy, National Nuclear Security Administration under Contract DE-AC52-07NA27344.

VIII. REFERENCES

[1] V. D. Ryzhikov, S. V. Naydenov, G. M. Onyshchenko, L. A. Piven, T. Pochet, and C. F. Smith, “Multi-layer fast neutron detectors based on composite heavy-oxide scintillators for detection of illegal nuclear materials,” *Nucl. Instrum. Methods Phys. Res. Sect. Accel. Spectrometers Detect. Assoc. Equip.*, vol. 903, pp. 287–296, Sep. 2018, DOI: 10.1016/j.nima.2018.06.074.

[2] J. Allison *et al.*, “Recent developments in Geant 4,” *Nucl. Instrum. Methods Phys. Res. Sect. Accel. Spectrometers Detect. Assoc. Equip.*, vol. 835, pp. 186–225, Nov. 2016, DOI: 10.1016/j.nima.2016.06.125.

[3] R. Brun and F. Rademakers, “ROOT — An object oriented data analysis framework,” *Nucl. Instrum. Methods Phys. Res. Sect. Accel. Spectrometers Detect. Assoc. Equip.*, vol. 389, no. 1–2, pp. 81–86, Apr. 1997, DOI: 10.1016/S0168-9002(97)00048-X.

[4] V. D. Ryzhikov, S. V. Naydenov, T. Pochet, G. M. Onyshchenko, L. A. Piven, and C. F. Smith, “Advanced Multilayer Composite Heavy-Oxide Scintillator Detectors for High-Efficiency Fast Neutron Detection,” *IEEE Trans. Nucl. Sci.*, vol. 65, no. 9, pp. 2547–2553, Sep. 2018, DOI: 10.1109/TNS.2018.2825642.

[5] “ENDF: Evaluated Nuclear Data File.” [Online]. Available: https://www-nds.iaea.org/exfor/endf.htm. [Accessed: 15-Jan-2019].

[6] E. Dietz-Laursonn, “Peculiarities in the Simulation of Optical Physics with Geant4,” *ArXiv161205162 Phys.*, Dec. 2016.

[7] “Geant4 Book For Application Developers — Book For Application Developers 10.5 documentation.” [Online]. Available: http://geant4-userdoc.web.cern.ch/geant4-userdoc/UsersGuides/ForApplicationDeveloper/html/index.html. [Accessed: 21-Feb-2019].

[8] C. Domingo-Pardo *et al.*, “New measurement of neutron capture resonances in Bi 209,” *Phys. Rev. C*, vol. 74, no. 2, Aug. 2006, DOI: 10.1103/PhysRevC.74.025807.